[Research Paper] 대한금속 · 재료학회지 (*Korean J. Met. Mater.*), Vol. 60, No. 5 (2022) pp.384-390
DOI: 10.3365/KJMM.2022.60.5.384

Preparation and Investigation of Thermoelectric Properties of Cu_3SbS_4-Cu_3SbSe_4 Solid Solutions

Go-Eun Lee and Il-Ho Kim*

Department of Materials Science and Engineering, Korea National University of Transportation, Chungju 27469, Republic of Korea

Abstract: Cu-based ternary chalcogenides composed of earth-abundant and nontoxic elements are considered promising thermoelectric materials, although there are few reports on them. In our previous studies, optimal mechanical alloying (MA) and hot pressing (HP) were used to synthesize Cu_3SbS_4 (famatinite) and Cu_3SbSe_4 (permingeatite). In this study, solid solutions of $Cu_3SbS_{4-y}Se_y$ (y = 0–4) were prepared using MA and HP. X-ray diffraction and Rietveld refinement confirmed the formation of Cu_3SbS_4-Cu_3SbSe_4 solid solutions. The variation in lattice constants with Se content followed Vegard's law. As the Se content increased, the carrier concentration and mobility increased. All the specimens exhibited *p*-type conduction, showing positive Hall and Seebeck coefficients. As the Se content increased, the Seebeck coefficient decreased due to an increase in carrier concentration, while the power factor of the solid solutions was not enhanced compared with that of the end compounds. $Cu_3SbS_{2.4}Se_{1.6}$ exhibited the lowest lattice thermal conductivities of 0.84 $Wm^{-1}K^{-1}$ at 323 K and 0.56 $Wm^{-1}K^{-1}$ at 623 K because of phonon scattering (alloying scattering) caused by the formation of the solid solutions. In addition, the thermal conductivity was less than 0.8 $Wm^{-1}K^{-1}$ at 623 K. This was attributed to the phonon scattering (boundary scattering) caused by several grain boundaries introduced during MA. As the Se content increased, the dimensionless figure of merit gradually increased from 0.14 to 0.39 at 623 K.

(Received 23 December, 2021; Accepted 19 January 2022)

Keywords: thermoelectric; famatinite; permingeatite; solid solution; mechanical alloying

1. INTRODUCTION

Sustainable alternative energy solutions need to be developed to prevent energy and environmental crises caused by increasing global energy consumption. Thermoelectric technologies, which can directly convert waste heat to electrical energy, have long attracted attention as a promising alternative energy solution. The conversion efficiency of thermoelectric devices is described by a dimensionless figure of merit ($ZT = \sigma\alpha^2 T\kappa^{-1}$), where σ: electrical conductivity, α: Seebeck coefficient, T: temperature in Kelvin, and κ: thermal conductivity). Therefore, to achieve a high ZT value, a high power factor ($\sigma\alpha^2$) and low thermal conductivity are required.

Recently, eco-friendly materials composed of nontoxic and earth-abundant elements have been extensively explored for thermoelectric devices. Among them, Cu-based ternary chalcogenides have received significant attention as promising materials for photovoltaic and thermoelectric applications [1-3]. Two of these, Cu_3SbS_4 (famatinite; space group $I\bar{4}2\,m$) and Cu_3SbSe_4 (permingeatite; space group $I\bar{4}2\,m$) are considered promising *p*-type thermoelectric materials in the intermediate-temperature range because of their narrow bandgap energy and low thermal conductivity [4,5]. Typically, two compounds with the same crystal structure can easily form a solid solution. This process is particularly suitable for thermoelectric materials when the guest atoms scatter phonons rather than electrons [6]. Cu_3SbS_4 and Cu_3SbSe_4 have a zinc-blende-type tetragonal structure, and they can form substitutional solid solutions because the differences in their atomic radii, and electronegativity between S^{2-} and Se^{2-}, are small. The substitution of Se for S causes lattice distortion due to different bonding interactions [7] and affects the effective mass of the valence bands [8]. Subsequent changes in the

- 이고은: 박사과정, 김일호: 교수
*Corresponding Author: Il-Ho Kim
[Tel: +82-43-841-5387, E-mail: ihkim@ut.ac.kr]

thermal and electrical properties and crystal lattice can be expected following the formation of solid solutions.

The melting method generally used to synthesize chalcogenides requires slow heating/cooling rates because of the high vapor pressure of the chalcogen elements and the long annealing time required for phase transformation and homogenization [6,7,9]. As a solution to the aforementioned problems, Cu_3SbS_4-Cu_3SbSe_4 solid solutions can be synthesized via mechanical alloying (MA) (high-energy ball milling) at room temperature. In our previous studies [10,11], Cu_3SbS_4 and Cu_3SbSe_4 powders were synthesized using MA and consolidated using hot pressing (HP), and the optimal conditions of MA (at 350 rpm for 12 h) and HP (at 623 K and 70 MPa for 2 h) were determined. In this study, solid solutions of $Cu_3SbS_{4-y}Se_y$ (y = 0–4) were prepared using MA and HP as a solid-state method, and their thermoelectric properties were investigated.

2. EXPERIMENTAL PROCEDURE

Solid solutions of $Cu_3SbS_{4-y}Se_y$ (y = 0, 0.8, 1.6, 2.4, 3.2, and 4), Cu (purity 99.9%, < 45 μm), Sb (purity 99.999%, < 75 μm), S (purity 99.99%, < 75 μm), and Se (purity 99.9%, < 10 μm) were weighed according to the corresponding stoichiometric composition. The mixed powders were loaded into a hardened steel jar with steel balls in an Ar atmosphere. MA was conducted using a planetary ball mill to synthesize the solid solutions, and then HP was performed to consolidate the synthesized powders.

X-ray diffraction (XRD; D2-PHASER, Bruker) was conducted to identify the phases of the MA powders and HP compacts, and Rietveld refinement (TOPAS, Bruker) was performed to estimate their lattice constants. Thermogravimetry and differential scanning calorimetry (TG-DSC; TG/DSC1, Mettler Toledo) were employed to analyze the mass changes and phase transformations of the MA powders and HP compacts. Field-emission scanning electron microscopy (FESEM; JSM-7610F, JEOL,) was used to observe the microstructures. Energy-dispersive spectroscopy (EDS; X-Max50, Oxford) was used to analyze the compositions and elemental distributions with the following energy levels: Cu L-series (0.930 eV), Se L-series (1.379 eV), S K-series (2.307 eV), and Sb L-series (3.604 eV).

The van der Pauw method was used to examine the Hall coefficient, carrier concentration, and mobility. ZEM-3 (ADVANCE RIKO) equipment was employed to measure the Seebeck coefficient and electrical conductivity. A laser flash TC-9000H (ADVANCE RIKO) system was used to measure thermal diffusivity, and then the thermal conductivity was estimated from the theoretical density and specific heat. Finally, the thermoelectric power factor and figure of merit were evaluated.

3. RESULTS AND DISCUSSION

The XRD patterns of the MA powders and HP specimens of $Cu_3SbS_{4-y}Se_y$ are shown in Fig. 1. All the solid solutions were prepared without secondary phases via the MA-HP process. As the Se content increased, all of the diffraction peaks shifted to lower diffraction angles. This indicated that

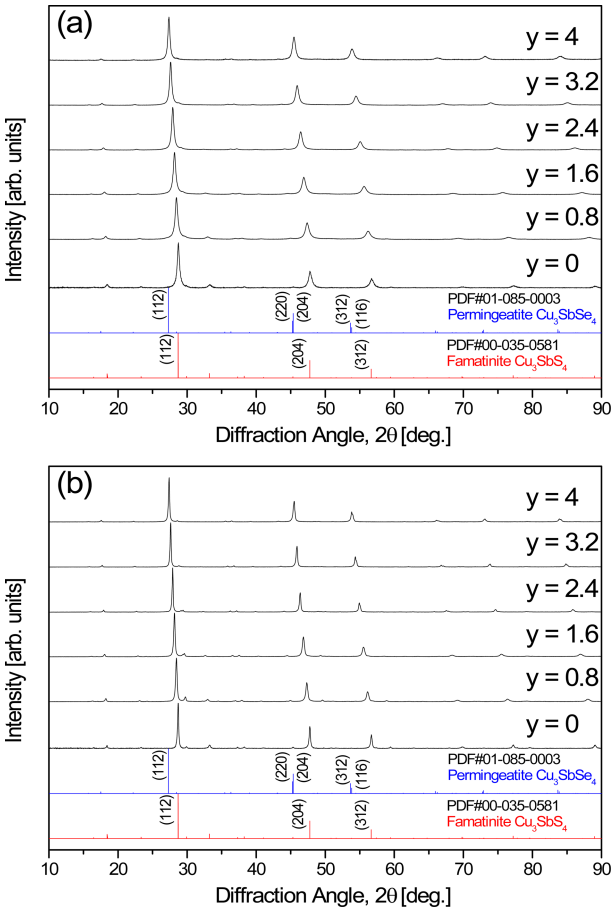

Fig. 1. XRD patterns for the (a) synthetic powders and (b) sintered specimens of $Cu_3SbS_{4-y}Se_y$.

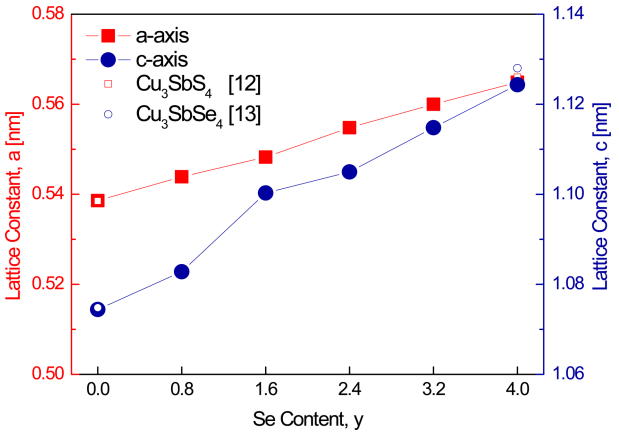

Fig. 2. Variations in the lattice constants of the $Cu_3SbS_{4-y}Se_y$ solid solutions.

the lattice constants were increased by the formation of substitutional solid solutions of Cu_3SbS_4 (PDF# 00-035-0518, famatinite) and Cu_3SbSe_4 (PDF# 01-085-0003, permingeatite).

The estimated lattice constants of the $Cu_3SbS_{4-y}Se_y$ solid solutions are shown in Fig. 2. Cu_3SbS_4 had lattice constants of a = 0.539 nm and c = 1.074 nm, and Cu_3SbSe_4 had lattice constants of a = 0.565 nm and c = 1.124 nm. Sugaki et al. [12] reported lattice constants of a = 0.539 nm and c = 1.075 nm for Cu_3SbS_4, and Pfitzner [13] reported lattice constants of a = 0.566 nm and c = 1.128 nm for Cu_3SbSe_4. Because the ionic radius of Se (0.198 nm) is larger than that of S (0.184 nm) [14], the lattice constants of the solutions increased almost linearly with increasing Se content, according to Vegard's law. This linear increase in lattice constants indicates that Se atoms were dissolved successfully into the S sites.

The results of the TG-DSC analyses of the hot-pressed $Cu_3SbS_{4-y}Se_y$ solid solutions are shown in Fig. 3. In previous studies [10,11], the melting points of Cu_3SbS_4 and Cu_3SbSe_4 were determined to be 823 K and 734 K, respectively, and no phase transformation or decomposition was observed at these temperatures. In this study, the melting points of $Cu_3SbS_{4-y}Se_y$ decreased with increasing Se content (y): the melting points were 818 K for y = 0.8, 778 K for y = 1.6, 752 K for y = 2.4, and 743 K for y = 3.2. As shown in Fig. 3(a), mass loss occurred at temperatures above the melting points, which was mainly due to the volatilization of the chalcogen

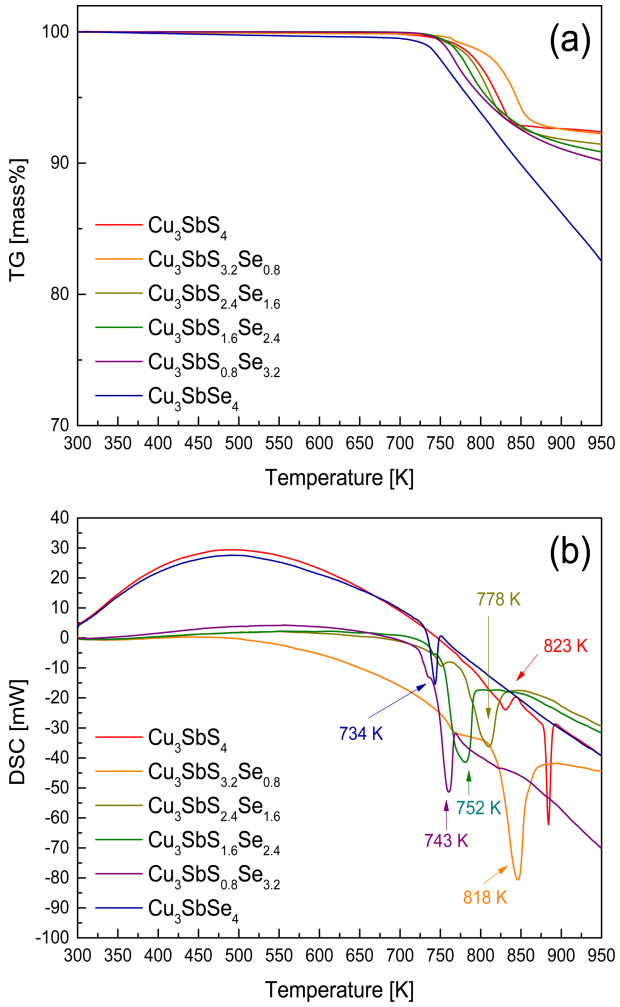

Fig. 3. (a) TG and (b) DSC analyses for the hot-pressed $Cu_3SbS_{4-y}Se_y$.

elements. For Cu_3SbS_4, the large endothermic peak at 880 K corresponds to the melting point of skinnerite (Cu_3SbS_3) [10].

Figure 4 displays FESEM images of the polished (backscattered electron mode) and fractured surfaces of the $Cu_3SbS_{4-y}Se_y$. All the specimens contained only a few pores, and their relative densities were higher than 97.8%. The theoretical density of famatinite (Cu_3SbS_4) was reported to be 4.64 gcm^{-3} [15], and that of permingeatite (Cu_3SbSe_4) was reported to be 5.86 gcm^{-3} [16]. The theoretical densities of the $Cu_3SbS_{4-y}Se_y$ solid solutions ($0.8 \le y \le 3.2$) were simply assumed and estimated using the rule of mixtures with Cu_3SbS_4 and Cu_3SbSe_4. The microstructures showed no significant differences despite the various Se contents. The actual compositions were similar to the nominal

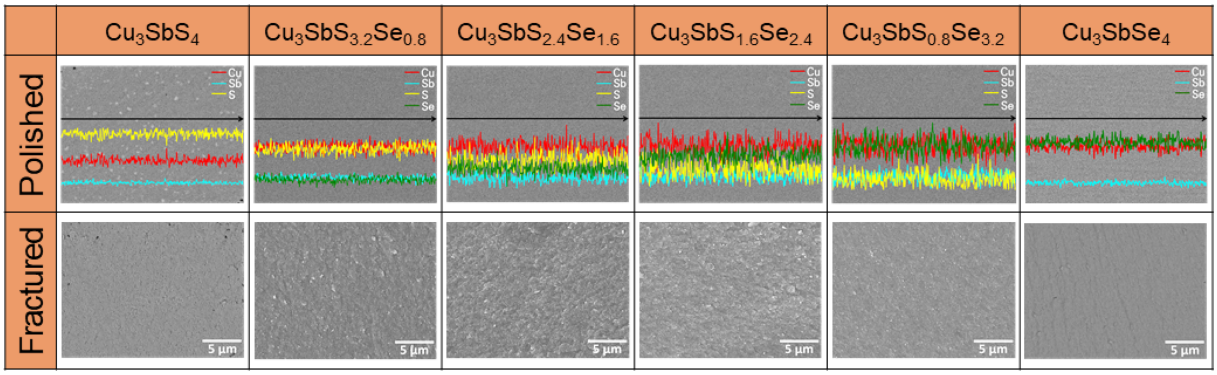

Fig. 4. FESEM images of the polished and fractured surfaces of $Cu_3SbS_{4-y}Se_y$.

Table 1. Chemical compositions, relative densities, and Lorenz numbers of $Cu_3SbS_{4-y}Se_y$.

Composition		Relative density [%]	Lorenz number [10^{-8} V^2K^{-2}]
Nominal	Actual		
Cu_3SbS_4	$Cu_{3.13}Sb_{1.04}S_{3.83}$	99.5	1.51
$Cu_3SbS_{3.2}Se_{0.8}$	$Cu_{3.19}Sb_{0.97}S_{3.04}Se_{0.80}$	100.0	1.52
$Cu_3SbS_{2.4}Se_{1.6}$	$Cu_{3.17}Sb_{0.97}S_{2.25}Se_{1.61}$	99.9	1.53
$Cu_3SbS_{1.6}Se_{2.4}$	$Cu_{3.13}Sb_{0.96}S_{1.50}Se_{2.40}$	99.5	1.54
$Cu_3SbS_{0.8}Se_{3.2}$	$Cu_{3.13}Sb_{0.94}S_{0.77}Se_{3.16}$	98.8	1.54
Cu_3SbSe_4	$Cu_{3.44}Sb_{0.67}Se_{3.89}$	97.8	1.57

compositions (Table 1), and all the constituent elements were observed to be homogeneously distributed in the EDS line scans.

Figure 5 shows the electrical conductivity of $Cu_3SbS_{4-y}Se_y$. The positive temperature dependence of the electrical conductivity indicates nondegenerate semiconductor behavior. The temperature dependence of the electrical conductivity decreased with increasing Se content, but the electrical conductivity increased at a constant temperature. To elucidate the change in electrical conductivity, the carrier concentration and mobility were measured (Fig. 6). Cu_3SbS_4 had a carrier concentration of 2.2×10^{18} cm^{-3} and a mobility of 1.6 $cm^2V^{-1}s^{-1}$, whereas Cu_3SbSe_4 had a carrier concentration of 5.2×10^{18} cm^{-3} and a mobility of 49.9 $cm^2V^{-1}s^{-1}$. As the Se content increased, the carrier concentration and mobility increased, and thus the electrical conductivity increased.

On the other hand, the Seebeck coefficient decreased with increasing Se content, as shown in Fig. 7. According to the Pisarenko relation [17], the Seebeck coefficient decreased with increasing Se content, owing to the increase in the

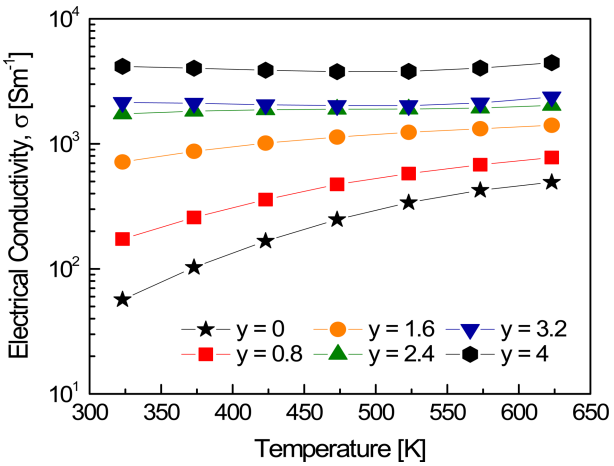

Fig. 5. Electrical conductivity of $Cu_3SbS_{4-y}Se_y$.

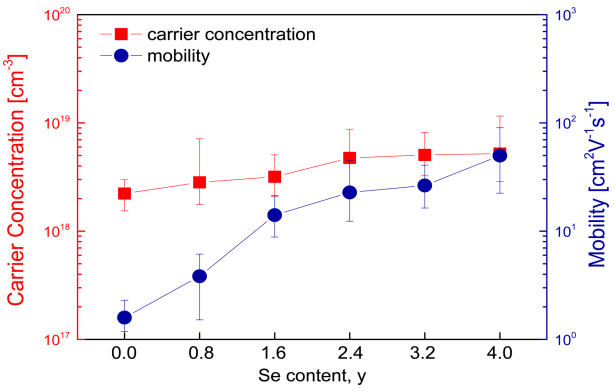

Fig. 6. Electronic transport properties of $Cu_3SbS_{4-y}Se_y$.

carrier concentration. The intrinsic carrier concentration (n_i) is closely related to the bandgap energy, according to the following equation [18]: $n_i = CT^{3/2}\exp[-E_g/2k_BT]$ (C: constant, E_g: bandgap, and k_B: Boltzmann constant). Cho et al. [19] reported that as the Te content increased in SnSe-SnTe solid

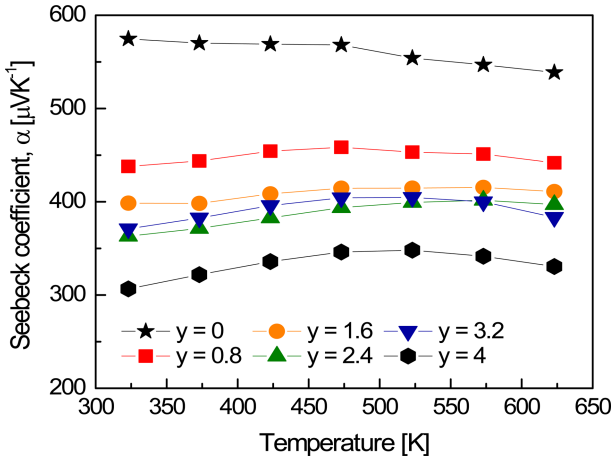

Fig. 7. Seebeck coefficient of $Cu_3SbS_{4-y}Se_y$.

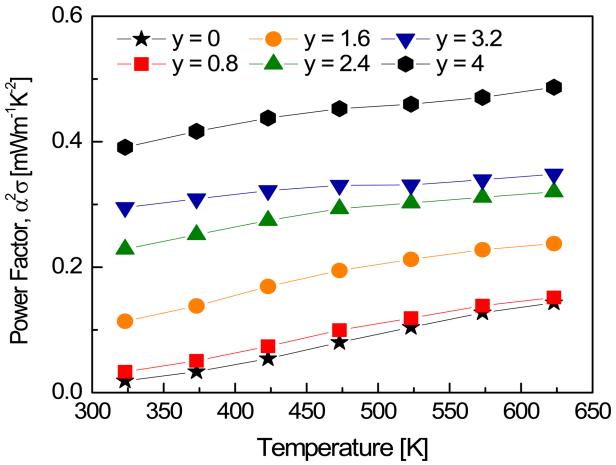

Fig. 8. Power factor of $Cu_3SbS_{4-y}Se_y$.

solutions, the Seebeck coefficient decreased due to the increase in carrier concentration caused by the reduction in bandgap. The bandgap of Cu_3SbS_4 ranges from 0.47 eV to 0.9 eV [20,21], and that of Cu_3SbSe_4 has been reported to be ~0.29 eV [4]. Therefore, the bandgap was decreased by the formation of a Cu_3SbS_4-Cu_3SbSe_4 solid solution. As the intrinsic carrier concentration increased, it in turn changed the electrical conductivity and Seebeck coefficient. As the Se content increased, the power factor values of the solid solutions lay between those of Cu_3SbS_4 and Cu_3SbSe_4 (Fig. 8). This suggests that optimization of the carrier concentration through doping is required to improve the power factor.

Figure 9 shows the thermal conductivity of $Cu_3SbS_{4-y}Se_y$. The thermal conductivity is the result of contributions from

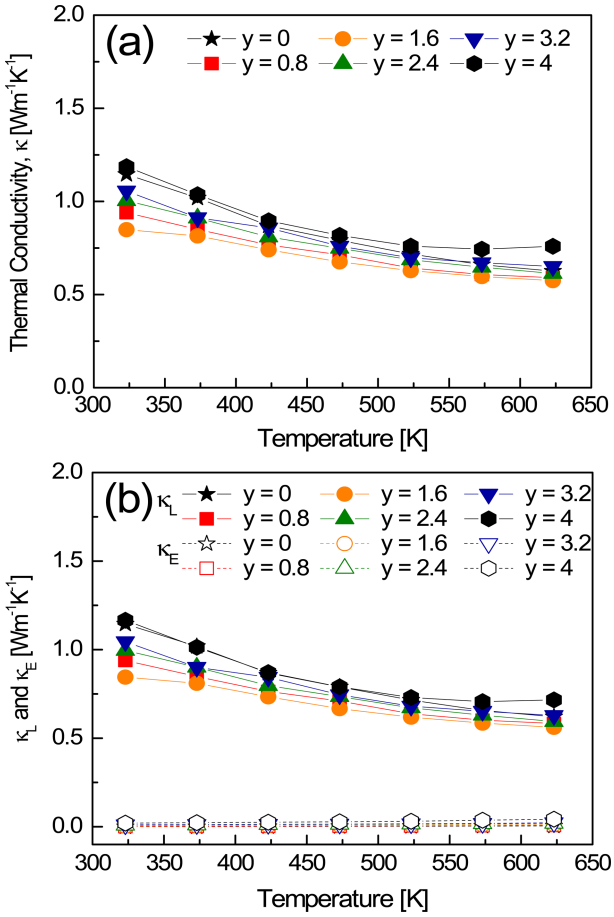

Fig. 9. Thermal conductivity of $Cu_3SbS_{4-y}Se_y$; (a) total thermal conductivity and (b) lattice and electronic thermal conductivities.

the charge carrier transport (κ_E, electronic thermal conductivity) and lattice vibrations (κ_L, lattice thermal conductivity). The Wiedemann–Franz law ($\kappa_E = L\sigma T$) was applied to separate the electronic thermal conductivity; the temperature-dependent Lorenz number (L) was obtained using the equation [22], $L = 1.5 + \exp[-|\alpha|/116]$. In this study, the ranges of the Lorenz number were $(1.51–1.57) \times 10^{-8}$ V^2K^{-2} at 323 K and $(1.51–1.56) \times 10^{-8}$ V^2K^{-2} at 623 K. The Lorenz number increased slightly with increasing Se content. The estimated Lorenz numbers at 323 K are summarized in Table 1. The Lorenz number has a theoretical range of $(1.45–2.44) \times 10^{-8}$ V^2K^{-2} [23], and the lower values indicate nondegenerate semiconductor behavior (the higher values indicate degenerate semiconductor or metallic behavior). This indicates that $Cu_3SbS_{4-y}Se_y$ is a nondegenerate semiconductor.

The thermal conductivities of the solid solutions were lower than that of $Cu_3Sb(S/Se)_4$, and this was attributed to

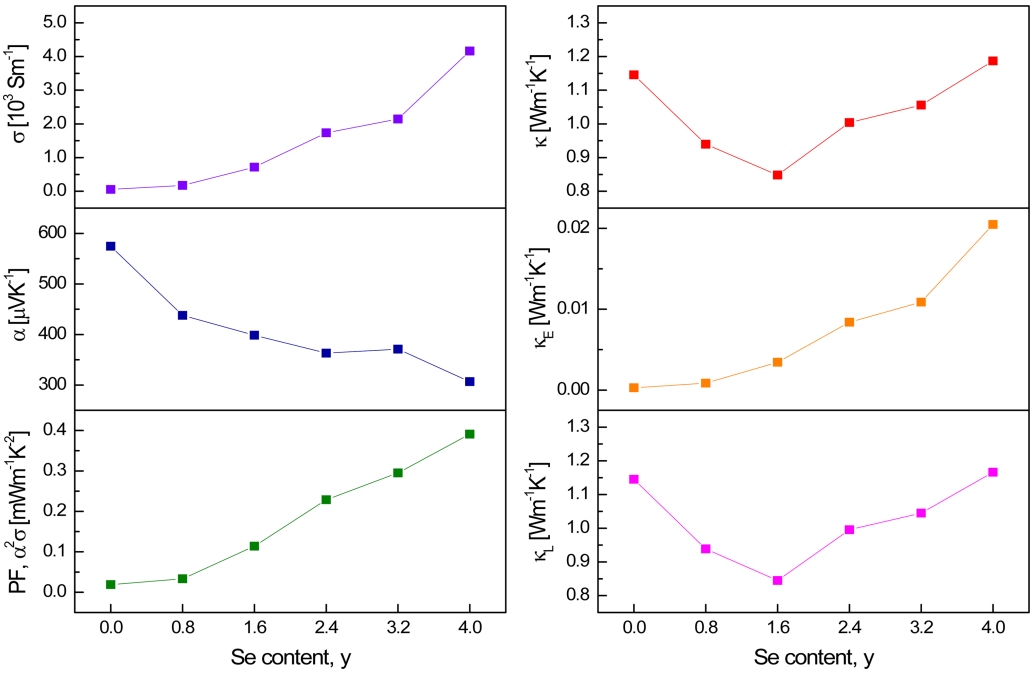

Fig. 10. Variations of the thermoelectric properties at 323 K with Se content for $Cu_3SbS_{4-y}Se_y$.

reduced lattice thermal conductivity resulting from lattice distortion. There was little contribution from the electronic thermal conductivity, because of the poor electrical conductivity. In addition, the thermal conductivity was less than 0.8 $Wm^{-1}K^{-1}$ at 623 K. These values were much lower than the values of 1.8–2.2 $Wm^{-1}K^{-1}$ reported for the $Cu_3SbS_{4-y}Se_y$ (y = 0.8, 1.2) solid solutions prepared via the melting process [24]. This can be attributed to the enhanced phonon scattering, following the introduction of numerous grain boundaries during MA.

Figure 10 shows the variation in thermoelectric properties at 323 K with Se content for $Cu_3SbS_{4-y}Se_y$. As mentioned previously, as the Se content (i.e., Cu_3SbSe_4 content) increased, the intrinsic carrier concentration increased, due to the reduction in bandgap energy. As a result, the electrical conductivity increased, while the Seebeck coefficient decreased, resulting in an increase in the power factor. The electronic thermal conductivity increased with increasing Se content. However, the specimen with y = 1.6 exhibited the lowest lattice thermal conductivity, and thus, the lowest thermal conductivity. This was due to the alloying effect (phonon scattering) caused by the difference in atomic mass between S (32.07 $gmol^{-1}$) and Se (79.86 $gmol^{-1}$) [25,26]. The

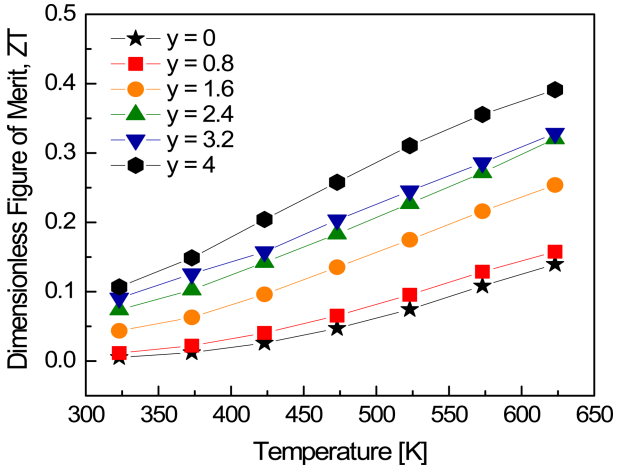

Fig. 11. Dimensionless figure of merit for $Cu_3SbS_{4-y}Se_y$.

lowest lattice thermal conductivity was 0.84 $Wm^{-1}K^{-1}$ for $Cu_3SbS_{2.4}Se_{0.16}$, which was mainly attributed to the enhanced phonon scattering caused by strain field fluctuations due to the differences in atomic radius and mass.

Figure 11 shows the *ZT* values of $Cu_3SbS_{4-y}Se_y$. As the temperature and Se content increased, the *ZT* values increased. All the solid solutions ($0.8 \le y \le 3.2$) exhibited *ZT* values between those of the end compounds (y = 0 or y = 4) without further improvement, despite the reduction in lattice

thermal conductivity. However, the formation of solid solutions did effectively decrease thermal conductivity, and controlled the electrical properties. The thermoelectric performance was expected to be improved by maximizing the power factor, by optimizing the carrier concentration.

4. CONCLUSIONS

Solid solutions of $Cu_3SbS_{4-y}Se_y$ (y = 0–4) were prepared using MA and HP. The lattice constants increased linearly with increasing Se content, indicating the successful formation of $Cu_3SbS_{4-y}Se_y$ solid solutions. The signs and values of the Hall and Seebeck coefficients confirmed *p*-type conduction and nondegenerate semiconductor characteristics. As the Se content increased, the carrier concentration and mobility increased; as a result, electrical conductivity increased, while the Seebeck coefficient decreased. Consequently, the power factor increased. The thermal conductivity was lowered by the formation of the solid solutions, and the contribution (phonon scattering due to the lattice distortion) of the lattice thermal conductivity was dominant. These results confirmed the effect of the solid solution on thermal conductivity, and doping will be required to improve the thermoelectric performance of $Cu_3SbS_{4-y}Se_y$ solid solutions in further studies.

ACKNOWLEDGMENT

This study was supported by the Basic Science Research Capacity Enhancement Project (National Research Facilities and Equipment Center) through the Korea Basic Science Institute funded by the Ministry of Education (Grant No. 2019R1A6C1010047).

REFERENCES

1. J. Li, X. Han, J. Li, Y. Zhao, and C. Fan, *Phys. Stat. Sol. B* **254**, 1600608 (2017).
2. S. Y. Kim, J. H. Pi, G. E. Lee, and I. H. Kim, *Korean J. Met. Mater.* **58**, 340 (2020).
3. R. Bhardwaj, A. Bhattacharya, K. Tyagi, B. Gahtori, N. S. Chauhan, S. Bathula, S. Auluck, and A. Dhar, *Mater. Res. Bull.* **113**, 38 (2019).
4. T. R. Wei, H. Wang, Z. M. Gibbs, C. F. Wu, G. J. Snyder, and J. F. Li, *J. Mater. Chem. A* **2**, 13527 (2014).
5. D. Chen, Y. Zhao, Y. Chen, T. Lu, Y. Wang, J. Zhou, and Z. Liang, *Adv. Electron. Mater.* **2**, 1500473 (2016).
6. E. J. Skoug, J. D. Cain, D. T. Morelli, M. Kirkham, P. Majsztrik, and E. Lara-Curzio, *J. Appl. Phys.* **110**, 023501 (2011).
7. L. Min, P. Ying, X. Li, and J. Cui, *J. Phys. D* **53**, 075304 (2019).
8. K. Chen, *Ph.D. Thesis*, Queen Mary University of London, UK (2016).
9. T. Tanishita, K. Suekuni, H. Nishiate, C. H. Lee, and M. Ohtaki, *Phys. Chem. Chem. Phys.* **22**, 2081 (2020).
10. G. E. Lee, J. H. Pi, and I. H. Kim, *J. Electron. Mater.* **49**, 2781 (2020).
11. G. E. Lee and I. H. Kim, *Materials* **14**, 1116 (2021).
12. A. Sugaki, A. Kitakaze, and Y. Shimizu, *Sci. Rep, Tohoku Univ. 3rd Ser.* **15**, 257 (1982).
13. A. Pfitzner, Z. Anorg. Allg. Chem. **621**, 685 (1995).
14. D. Li, H. W. Ming, J. M. Li, B. Jabar, W. Xu, J. Zhang, and X. Y. Qin, *ACS Appl. Mater. Interfaces* **12**, 3886 (2020).
15. O. Madelung, Semiconductors: Data Handbook, *3rd* ed., Springer, Berlin (2004).
16. Y. Li, X. Qin, D. Li, X. Li, Y. Liu, J. Zhang, C. Song, and H. Xin, *RSC Adv.* **5**, 31399 (2015).
17. J. P. Heremans, B. Wiendlocha, and A. M. Chamoire, *Energy Environ. Sci.* **5**, 5510 (2012).
18. J. Jimenez and J. W. Tomm, Spectroscopic Analysis of Optoelectronic Semiconductors, Springer, Switzerland (2016).
19. J. Y. Cho, M. Siyar, W. C. Jin, E. Hwang, S. H. Bae, S. H. Hong, M. Kim, and C. Park, *Materials* **12**, 3854 (2019).
20. C. Coughlan, M. Ibáñez, O. Dobrozhan, A. Singh, A. Cabot, and K. M. Ryan, *Chem. Rev.* **117**, 5865 (2017).
21. Y. Goto, Y. Sakai, Y. Kamihara, and M. Matoba, *J. Phys. Soc. Jpn.* **84**, 044706 (2015).
22. H. S. Kim, Z. M. Gibbs, Y. Tang, H. Wang, and G. J. Snyder, *APL Mater.* **3**, 041506 (2015).
23. S. G. Kwak, J. H. Pi, G. E. Lee, and I. H. Kim, *Korean J. Met. Mater.* **58**, 272 (2020).
24. E. J. Skoug, J. D. Cain, and D. T. Morelli, *Appl. Phys. Lett.* **98**, 261911 (2011).
25. L. Chen, G. Jiang, Y. Chen, Z. Du, X. Zhao, T. Zhu, J. He, and T. M. Tritt, *J. Mater. Res.* **26**, 3038 (2011).
26. Asfandiyar, T. R. Wei, Z. Li, F. H. Sun, Y. Pan, C. F. Wu, M. U. Farooq, H. Tang, F. Li, B. Li, and J. F. Li, *Sci. Rep.* **7**, 43262 (2017).